

# THE DYNAMIC APERTURE OF THE LNLS UVX2 ELECTRON STORAGE RING

Liu Lin and L.Jahnel

Laboratório Nacional de Luz Síncrotron - LNLS/CNPq  
Caixa Postal 6192 - Campinas - SP - Brazil.

## Abstract

Beam dynamics studies of the LNLS 1.15 GeV UVX2 electron storage ring are described. The effect of magnetic multipole errors, alignment and excitation errors are discussed. A systematic study of the effect of resonances induced by sextupoles and the optimization of the dynamic aperture are carried out.

## 1. INTRODUCTION

The Brazilian Synchrotron Light Laboratory (LNLS) is designing and building a dedicated vacuum ultraviolet-soft X-ray radiation source. The photon beams will be provided by bending magnets and insertion devices (wigglers and undulators). The latest lattice version - UVX2 - is a six fold symmetric double bend achromat lattice operating with 1.15 GeV electrons<sup>[1]</sup>. Figure 1 illustrates one superperiod of the storage ring. Three meter long dispersion free straight sections are provided for insertion devices. Figure 2 shows the optical functions for the normal operation mode in one superperiod of the ring.

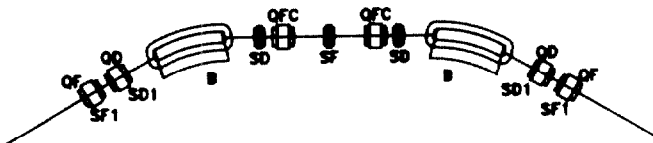


Figure 1: Lay-out of one superperiod of UVX2.

Such a dedicated storage ring must be optimized for small beam emittance. This lead us to use strong focussing lattices which produce large chromatic aberrations. The produced natural chromaticity,  $\xi_0 = \Delta v / (\Delta p/p)$  ( $\xi_{0x} = -8.17$  and  $\xi_{0y} = -9.70$  for UVX2 normal operation mode) must be compensated to prevent the beam from being killed by the fast head-tail instability. Two families of chromaticity correcting sextupoles, SF and SD, are introduced in the dispersive straight sections of the ring. These sextupoles, however, introduce non-linear perturbations which limit the dynamic aperture of the ring. Following an idea described elsewhere<sup>[2]</sup> we try to minimize the effects of these chromaticity correcting sextupoles by introducing two other sextupole families, SF1

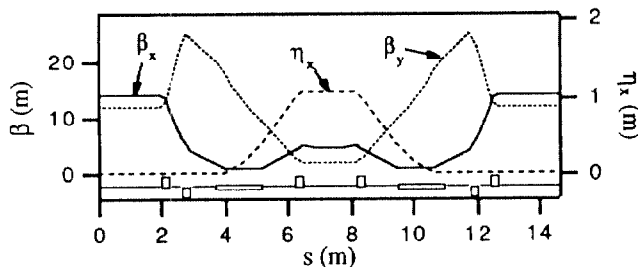


Figure 2: Schematic design of one superperiod of UVX2 and the focussing functions for the normal operation mode.

and SD1, located inside the quadrupole families QF and QD, respectively, in the non-dispersive straight section. See figure 1. The theoretical optimization of the sextupoles SF1 and SD1 is based, on one side, on the 'figure of merit' representing the non-linearities, the tune shift with amplitude (very appropriately described<sup>[3]</sup> by the Hamiltonian canonical perturbation theory); and, on the other side, on numerical tracking simulation using the code PatPet<sup>[4]</sup>.

## 2. TUNE SHIFT WITH AMPLITUDE

The tune shift with particle amplitude is often used to characterize the effects of the sextupole induced non-linear perturbations on the lattice. Its expression is derived in various references<sup>[3]</sup>. In the case where the linear tune is far from resonances, we have:

$$\begin{aligned}\Delta v_x &= A J_x + B J_y \\ \Delta v_y &= B J_x + C J_y\end{aligned}$$

where  $\Delta v_x$  and  $\Delta v_y$  are the horizontal and vertical tune shifts; A, B and C are coefficients determined only by the lattice (they are, thus, dependent on sextupole configuration), and  $J_x$  and  $J_y$  are action variables which are constants of the motion and depend on the initial conditions of the particle. For UVX2 normal operation mode, the linear horizontal and vertical tunes are  $v_x = 5.27$  and  $v_y = 2.17$ .

For UVX2 we have varied the strength of the two correcting sextupole families SF1 and SD1 to minimize the function  $F = w_a \cdot A^2 + w_b \cdot B^2 + w_c \cdot C^2$ , where  $w$  is a weight function. The calculations are done by a program which uses the minimization package Minuit<sup>[5]</sup>. The sextupoles are considered as thin lenses. Varying the weight function we can obtain different sextupole settings. Table I shows the values for the coefficients for some settings.

Table I: Coefficients for the tune shift with amplitude for three sextupole configurations.

	SF1=0 SD1=0	SF1=0.83 m <sup>-2</sup> SD1=-0.63 m <sup>-2</sup>	SF1=0.81 m <sup>-2</sup> SD1=-0.84 m <sup>-2</sup>
A	763	295	259
B	826	-238	229
C	584	987	149
A <sup>2</sup> +B <sup>2</sup> +C <sup>2</sup>	1.6E+06	1.1E+06	1.4E+05

## 3. NUMERICAL TRACKING SIMULATION

The approach described above considers only the effects of sextupoles on the lattice. To take into consideration other effects such as higher order multipole errors, excitation and alignment errors, numerical tracking simulation is performed with the code PatPet. The final choice of the strengths of SF1 and SD1 is based on the results of numerical simulation, the previous approach giving an initial estimate for the correcting sextupole values.

3.1 Multipole errors

The multipole ‘errors’ are the higher order terms of the real magnetic field expansion. In the analysis of the multipole components of our magnets we try to have in mind that they should reproduce the field within constructional and measurable field tolerances. We divide the multipole errors into two categories: systematic and random multipole errors. The systematic errors are those caused by the finite dimensions of the poles and are equal for every magnet of the same kind, whereas the random ones arise because of constructional tolerances and are different for each magnet. To obtain the systematic error values we have fitted a polynomial function (only with the symmetry-permitted terms) to the calculated field from Poisson<sup>[6]</sup>. The fitting is performed only within the physical limits of the ring (set by the vacuum chamber). Figure 4 shows the fitted (dashed curve) and the Poisson calculated fields for the dipole and quadrupole. The random errors are a compilation of worst-case values used in similar calculations in other projects [7] and estimates from mechanical gap parallelism tolerances. We have checked that the field will be reasonably represented within the physical area available for the beam. Table II shows the systematic multipole errors used for simulations and one standard deviation for the gaussian distribution of random multipole errors which are truncated at two sigmas.

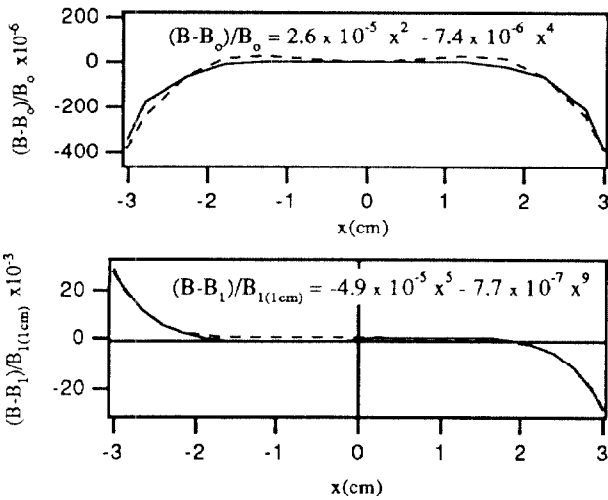


Figure 4: Magnetic field calculated by the code Poisson (full line) and the polynomial fitting (dashed line) for the dipole (top) and the quadrupole (bottom).

To save computer time we have analyzed the effects of the correcting sextupoles only with the systematic multipole errors. The random errors require many simulations with different seeds to get a statistical analysis. Dynamic aperture calculations for various settings of SF1 and SD1 were performed. We show in figure 5 the dynamic aperture for two sextupole settings: SF1 and SD1 off and with values that most enlarged the aperture (SF1=0.83 m<sup>-2</sup>, SD1=-0.63 m<sup>-2</sup>). After determining the setting of these correcting sextupoles, a simulation including both types of multipole errors plus excitation and alignment errors is performed for various seeds.

In all cases, simulation is done with physical limits for, as we stressed above, the magnetic field is only well represented by the multipolar expansion within these limits. The results are shown in the next section.

Table II: Magnetic multipole errors. The field is expanded as

$$B(x) = \sum_n \frac{1}{n!} \frac{\partial^n B}{\partial x^n} x^n = \sum_n B_n$$

n	Dipole $B_n/B_0^*$		Quadrupole $B_n/B_1^*$	
	Systematic	Random	Systematic	Random
1	-	$5 \times 10^{-5}$	-	-
2	$2.6 \times 10^{-5}$	$1 \times 10^{-4}$	-	$5 \times 10^{-4}$
3	-	$2 \times 10^{-5}$	-	$2 \times 10^{-4}$
4	$-7.4 \times 10^{-6}$	$1 \times 10^{-5}$	-	$6 \times 10^{-5}$
5	-	-	$-4.9 \times 10^{-5}$	$1 \times 10^{-5}$
9	-	-	$-7.7 \times 10^{-7}$	$4 \times 10^{-8}$

\*Values at x=1 cm.

It is interesting to see the phase space plots for particles near the edge of the dynamic aperture. Figure 6 shows such a plot, for the horizontal and vertical phase spaces, for a particle with amplitude near the limit of the dynamic aperture. These phase space plots are taken at the middle of the long insertion straight section for the machine with systematic multipole errors only. The tune diagram and action variables for successive turns are also shown in this figure.

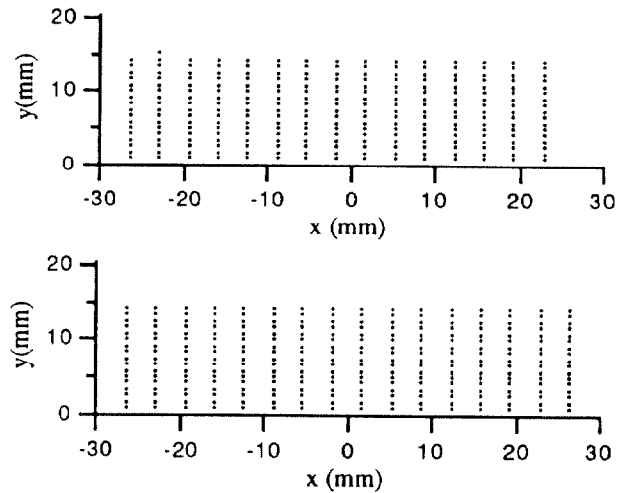


Figure 5: Dynamic aperture at the middle of the insertion straight for the machine with systematic multipole errors only. Physical limits are included. Top: SF1 and SD1 off. Bottom: SF1=0.83 m<sup>-2</sup> and SD1=-0.63 m<sup>-2</sup>.

3.2 Alignment and excitation errors

We have also defined random strength (excitation) and magnet alignment errors. The alignment errors are horizontal  $x$  and vertical  $y$  displacements and rotation  $\alpha$  about the longitudinal axis. Table III shows the assumed standard deviations for gaussian distributions of random errors, which are truncated at two sigmas. For the cases where excitation and alignment errors are included, tracking is done after closed orbit corrections. Errors in the alignment of position monitors are also included.

Table III : Alignment and strength random errors (one standard deviation) in magnetic elements.

$\langle \Delta x \rangle, \langle \Delta y \rangle$	0.2 mm
$\langle \Delta \alpha \rangle$	0.02 °
$\langle \Delta S/S \rangle$	0.1 %

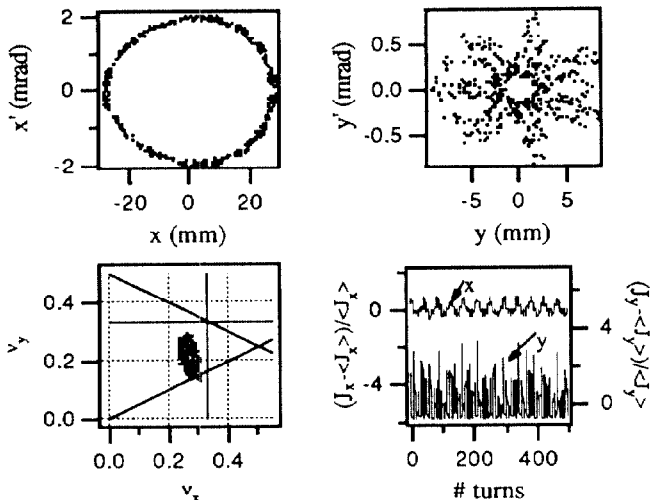


Figure 6: Top: horizontal and vertical phase space trajectories for a particle with amplitude near the limit of the dynamic aperture. These phase space plots are taken at the middle of the long insertion straight section for the machine with systematic multipole errors only. Bottom: Tune diagram (left) and relative action variables  $(J_x, J_y)/\langle J \rangle$  (right) for successive turns.

### 3.3 Results

We have found that the setting which most enlarged the dynamic aperture in the UVX2 normal operation mode is  $SF1=0.83 \text{ m}^{-2}$  and  $SD1=-0.63 \text{ m}^{-2}$ . The dynamic aperture calculations for this sextupole setting are presented in this section. Particles are tracked using PatPet for 500 turns. The calculations include systematic and random multipole errors, random excitation (strength) errors, random alignment errors, physical limits and particle momentum deviation.

The results for the dynamic aperture calculations at the middle of the long insertion straight are shown in figure 7. The hatched regions in these figures correspond to the uncertainty region of dynamic aperture for five different sets of random errors used.

The simulations show that in the presence of multipole and alignment errors the horizontal dynamic aperture may shrink to dimensions a bit smaller than the vacuum chamber aperture. This is still sufficiently large for injection and the inelastic gas scattering lifetime is still long enough (on the same order as the Touschek lifetime) to give an overall lifetime longer than 10 hours at 1.15 GeV.

## 4. CONCLUSIONS

The dynamic aperture of the LNL UVX2 storage ring has been optimized using two families of sextupoles in the non-dispersive straight section to minimize the tune shift with amplitude introduced by the chromaticity correction sextupoles. The values of these sextupoles are calculated by

minimizing the coefficients of the expression for the tune shift with amplitude derived using the Hamiltonian formalism. This calculation is used to obtain a first estimate to the values of the correcting sextupoles. The optimum set of values is found by numerical tracking (trial and error) including higher order systematic multipoles which are not taken into account in the previous formalism. We have found for UVX2 that even when other random errors are included the dynamic aperture remains sufficiently large.

We note that non-linear effects introduced by insertion devices, which can be very deleterious to the performance of the ring, were not taken into account. The next step for this dynamic aperture optimization study is to analyze the effect of these elements. Other operation modes should also be analysed.

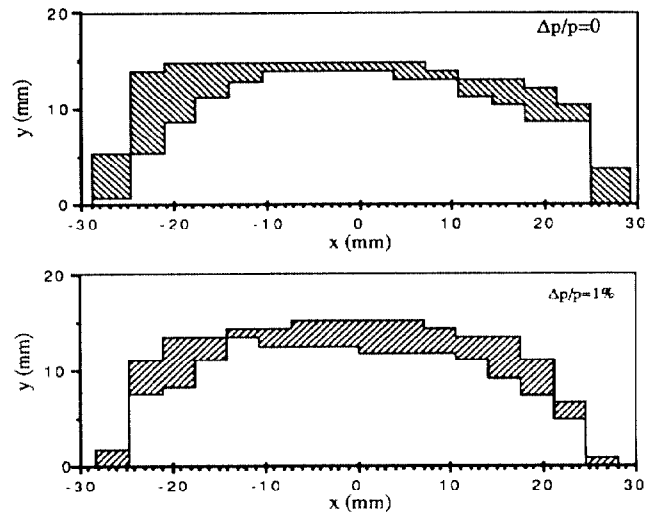


Figure 7: Dynamic aperture at the middle of the insertion straight for the machine with systematic and random multipole errors, strength and alignment errors for on-momentum particles (top) and 1 % momentum deviation (bottom).

## 5. REFERENCES

- [1] Liu Lin, L.Jahnel and P.Tavares, 'The LNL UVX2 Soft X-Ray Source', presented at this Conference.
- [2] See for example, E.A.Crosbie, 'Improvement of the Dynamic Aperture in Chasman Green Lattice Design Light Source Storage Rings'.
- [3] See for example, R.D.Ruth, 'Single Particle Dynamics in Circular Accelerators', AIP-CP 153, 152 and H. Zyngier, 'A Propos de L'Approximation du Second Ordre', LURE RT/91-10.
- [4] L.Emery, H.Wiedemann and J.Safranek, 'User's Guide for PatPet Version 88.2', SSRL ACD-NOTE 36.
- [5] F.James and M.Ross, 'Minuit-Long Write-up', CERN Computer Center, 1987.
- [6] Los Alamos Accelerator Group, 'User's Guide for the POISSON/Superfish Group of Codes', LA-UR-87-115 and 'Reference Manual for the POISSON/Superfish Group of Codes', LA-UR-87-126.
- [7] '1-2 GeV Synchrotron Radiation Source-Conceptual Design Report', LBL PUB-5172 Rev and S.Tazzari, Editor, 'Design Study for the Synchrotron Light Source', LNF-87/6(R).